Bioactive Materials 42 (2024) 573–586

Contents lists available at ScienceDirect

Bioactive Materials

journal homepage: www.keaipublishing.com/en/journals/bioactive-materials

Fc-empowered exosomes with superior epithelial layer transmission and lung distribution ability for pulmonary vaccination

Fan Meng [a,b,1], Haonan Xing [b,***,1], Jingru Li [b], Yingqi Liu [b], Li Tang [a], Zehong Chen [a,b], Xiran Jia [b], Zenglin Yin [b], Jing Yi [b], Mei Lu [c], Xiuli Gao [a,**], Aiping Zheng [b,*]

[a] School of Pharmaceutical Sciences & State Key Laboratory of Functions and Applications of Medicinal Plants & Microbiology and Biochemical Pharmaceutical Engineering Research Center of Guizhou Provincial Department of Education, Guizhou Medical University, Guiyang, 550025, China
[b] Institute of Pharmacology and Toxicology, Academy of Military Medical Sciences, Beijing, 100850, China
[c] Advanced Research Institute of Multidisciplinary Science, School of Life Science, School of Medical Technology (Institute of Engineering Medicine), Key Laboratory of Molecular Medicine and Biotherapy, Key Laboratory of Medical Molecule Science and Pharmaceutics Engineering Beijing Institute of Technology, Beijing, 100081, China

ARTICLE INFO

Keywords:
Fc
Exosomes
Vaccines
Mucosal immunity
SARS-CoV-2

ABSTRACT

Mucosal vaccines offer potential benefits over parenteral vaccines for they can trigger both systemic immune protection and immune responses at the predominant sites of pathogen infection. However, the defense function of mucosal barrier remains a challenge for vaccines to overcome. Here, we show that surface modification of exosomes with the fragment crystallizable (Fc) part from IgG can deliver the receptor-binding domain (RBD) of SARS-CoV-2 to cross mucosal epithelial layer and permeate into peripheral lung through neonatal Fc receptor (FcRn) mediated transcytosis. The exosomes F-L-R-Exo are generated by genetically engineered dendritic cells, in which a fusion protein Fc-Lamp2b-RBD is expressed and anchored on the membrane. After intratracheally administration, F-L-R-Exo is able to induce a high level of RBD-specific IgG and IgA antibodies in the animals' lungs. Furthermore, potent Th1 immune-biased T cell responses were also observed in both systemic and mucosal immune responses. F-L-R-Exo can protect the mice from SARS-CoV-2 pseudovirus infection after a challenge. These findings hold great promise for the development of a novel respiratory mucosal vaccine approach.

1. Introduction

The COVID-19 pandemic brought a great impact on society. Thanks to the rapid intervention of vaccines, human social activities have gradually returned to normal, marking the beginning of the post-epidemic era [1]. However, the threat of emerging and re-emerging infectious diseases still exists [2], and how we can do better when facing possible future pandemics remains a vital problem [3–7]. Vaccines are the most cost-effective approach to combating infectious diseases [8–11]. The research and development of vaccines underwent a revolution during the outbreak of COVID-19. Novel vaccine platforms utilizing characteristics of viruses were established, such as virus-like particle (VLP) vaccines, DNA vaccines, mRNA vaccines, and other related microorganism-based vaccines [12–17]. These vaccines have not only laid a solid foundation but have also made significant progress in optimizing vaccine design and understanding immune activation.

SARS-CoV-2 is an enveloped positive-strand RNA virus that initially binds to the angiotensin-converting enzyme 2 (ACE2) receptor in the host airway epithelium through the crown-like trimeric Spike (S) protein on the viral surface [18,19]. Mucosa serves as the first line of defense against the virus, providing scope for sterilizing immunity and allowing the immune system to recognize and eliminate the virus [20,21]. Accines administered through respiratory mucosa can elicit mucosal immune responses and thereby generate secretory immunoglobulin A

Peer review under responsibility of KeAi Communications Co., Ltd.
* Corresponding author.
** Corresponding author.
*** Corresponding author.
E-mail addresses: 1693921384@qq.com (F. Meng), xinghn010@foxmail.com (H. Xing), 374091696@qq.com (J. Li), 1549216916@qq.com (Y. Liu), li_tang_2023@163.com (L. Tang), 1158628148@qq.com (Z. Chen), 646099810@qq.com (X. Jia), 1127635382@qq.com (Z. Yin), yj13337211566@163.com (J. Yi), lumei@bit.edu.cn (M. Lu), gaoxl@gmc.edu.cn (X. Gao), apzheng@163.com (A. Zheng).
[1] These authors contributed equally: Fan Meng and Haonan Xing.

https://doi.org/10.1016/j.bioactmat.2024.08.015
Received 25 October 2023; Received in revised form 7 August 2024; Accepted 17 August 2024
2452-199X/© 2024 The Authors. Publishing services by Elsevier B.V. on behalf of KeAi Communications Co. Ltd. This is an open access article under the CC BY-NC-ND license (http://creativecommons.org/licenses/by-nc-nd/4.0/).

(sIgA) and tissue-resident memory (Trm) cells in the mucosal area [22,23]. Though mucosal vaccines can outperform injectable vaccination strategies in blocking both viral infection and transmission, significant hurdles exist for mucosal vaccine development, including incomplete knowledge of the nature of protective mucosal immune responses and the difficulties for vaccines to overcome the harsh environment of the mucosal barrier [24]. Given the protective nature of the mucosal barrier and its unique cellular composition, vaccine strategies should be specifically tailored rather than simply redeploying injectable vaccines [24,25]. For example, to enhance mucosal immune effects, Xiao et al. used cGAMP, mannan, and polyarginine to assemble nanoparticle vaccines under electrostatic interaction. Nasal administration of these vaccines induced mucosal IgA and IgG responses in bronchoalveolar lavage and nasal lavage [26]. To reduce the interference of barriers such as the mucus layer, Rakhra et al. covalently conjugated protein antigen and an amphipathic lipid, which was used as a lung mucosal vaccine [27]. This vaccine can bind to abundant albumin in the lung and be transported across the lung mucosal epithelium in a "hitchhiking" fashion by FcRn. The results showed that the vaccine under study resulted in a 25-fold increase in pulmonary Trm [27]. These studies represent some of the approaches that have successfully crossed the epithelial cells of the lung mucosa.

Extracellular vesicles (EVs), especially exosomes, which are released by almost all cells and have a diameter of 30–150 nm, play a crucial role in the transmission of information and exchange of materials between cells [28,29]. In recent years, exosomes derived from immune cells, such as macrophages, lymphocytes, and dendritic cells, have played an important role in regulating immune responses, antiviral immunity, and other immunological processes [30,31]. Specifically, DC-derived exosomes possess various advantages [32]. They carry co-stimulatory factors like CD80, CD86, MHC-I, and MHC-II, which endow them with the possibility of directly activating T cells. Meanwhile, by leveraging their homing abilities and the size effect of nano-scale particles, DC-derived exosomes exhibit significant advantages in delivery and immune activation, thereby enabling them to stimulate and regulate the immune system more effectively [33–36]. For example, the immunological efficacy of cross-dressing by exosomes was shown in experiments where pMHC-I complexes transferred by exosomes isolated from cultured human DCs could provide naive DCs with the capacity to efficiently prime melanoma-specific CD8 T cells in HLA-A2 transgenic mice [37].

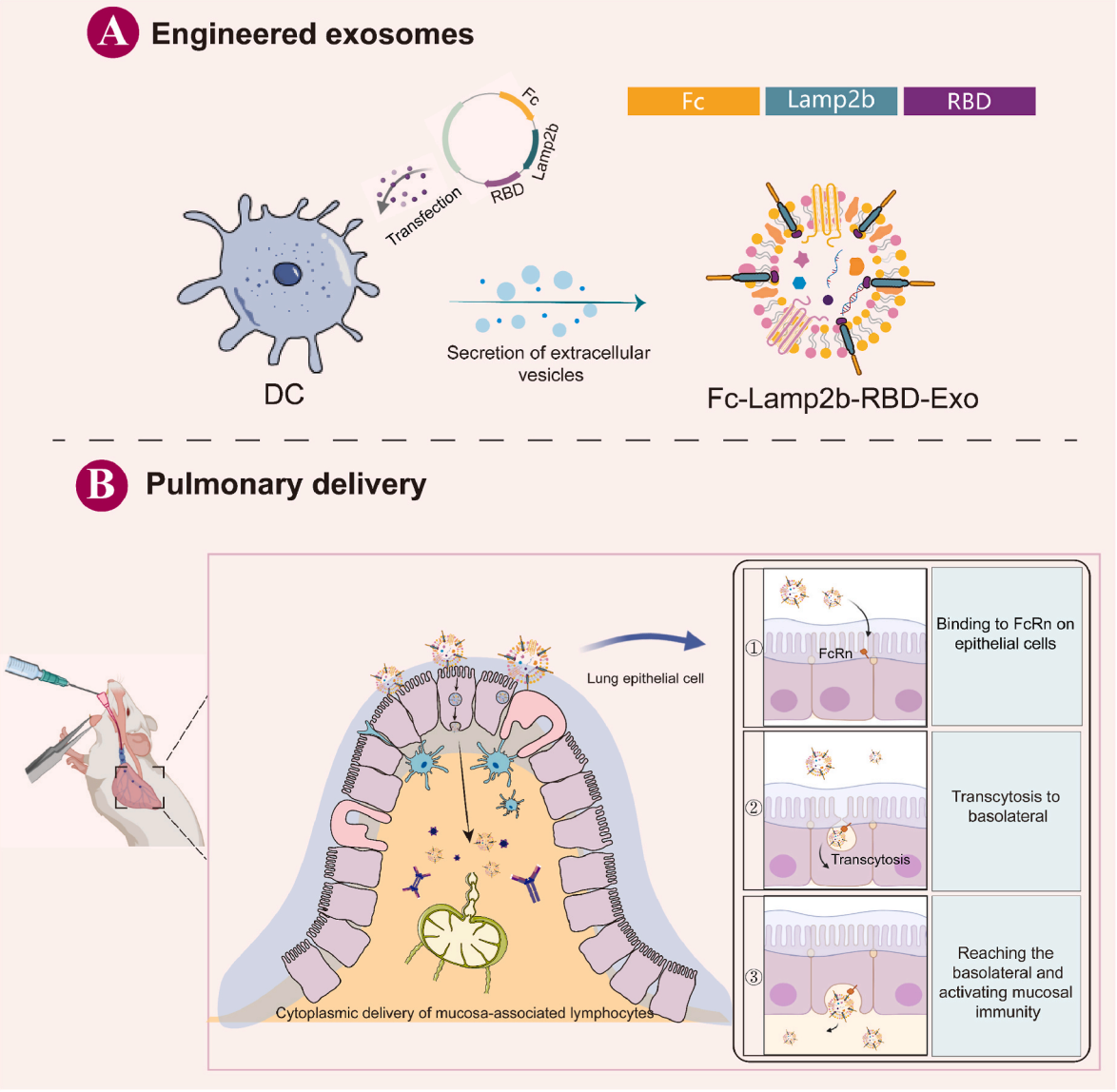

Fig. 1. Fc-lamp2b-RBD can induce mucosal-associated immunity in mice to neutralize SARS-CoV-2 and protect their lungs. **A.** The fusion gene was transfected to DC2.4 cells and the exosomes were extracted. **B.** The exosomes were administrated intratracheally and across the epithelial barrier via FcRn mediated transcytosis. This process induced both mucosal and systemic immune response in mice. The schematic was created using Biorender.

Furthermore, lung-derived exosomes have been explored as carriers for mRNA and protein drugs, which were delivered to the lungs of rodents and nonhuman primates through dry powder inhalation [38,39]. These mRNA-loaded cellular EVs induced a more potent immunoglobulin IgG and sIgA response than their counterparts, showcasing their potential for mucosal immunization.

In this study, we designed a novel chimeric protein by fusing Fc and the receptor binding domain of SARS-CoV-2 (RBD) to lysosomal-associated membrane protein 2b (Lamp2b). After transfecting DC2.4 cells with the plasmid encoding the fusion protein, the exosomes were decorated with Fc fragments on the ectodomain and RBD segments on the internal domain. Fc endowed the exosomes with good lung epithelial layer transmission ability via FcRn-mediated transcytosis [40], Lamp2b served as an exosome membrane anchor to increase the fusion protein density [41], and RBD played a vital role in activating the anti-viral immune response [42]. By engineering exosomes with this fusion protein, we hypothesize that the exosomes will elicit a better mucosal immune response by crossing the epithelial layer more effectively (Fig. 1).

2. Materials and methods

2.1. Cell culture

DC2.4 was derived from the American Type Culture Collection (ATCC), and the cells were cultured in Dulbecco's Modified Eagle Medium (DMEM) complete medium (with 10 % fetal bovine serum and 1 % penicillin/streptomycin). After the cells had grown to 80–90 % confluence, the culture supernatant was discarded, the cells were washed with PBS 1–2 times, and 2 mL of 0.25 % trypsin was added. After 30 s to 1 min of digestion, twice the amount of medium was added to terminate digestion. After centrifugation at 1000 rpm for 3 min, the supernatant was removed and the cells were resuspended in fresh complete medium, which was then distributed to a new dish.

2.2. Plasmid design and construction

First, the Fc sequence was obtained from the pUSE-higG1-FC2 plasmid and loaded into the plasmid vector pCDNA3.1 through enzyme digestion and ligation. The Lamp2b sequence (GenBank: AK304405.1) and RBD sequence (YP_009,724,390) were searched on the NCBI website. A linker (GGGGS)*3 was added between each protein, and a Flag tag protein was appended to the end of the sequence to create the Fc-Lamp2b-RBD plasmid. This process was performed by Tsingke Biotechnology Co., Ltd. Similarly, the Fc or RBD sequences were removed to form Lamp2b-RBD plasmids or Fc-Lamp2b plasmids.

2.3. Exosomes isolation and characterization

When the growth density of non-transfected DC2.4 cells reaches 80%–90 %, wash them twice with PBS. Then, add DMEM medium without serum and penicillin/streptomycin and culture for two days. Next, subject the DC2.4 cell supernatant to gradient centrifugation at 500*g* for 10 min, followed by 2000 g for 10 min, and finally 10,000 g for 30 min. This process helps remove any remaining cells and debris. After that, transfer the supernatant to a 100 kDa Amicon centrifugal filter device (Millipore Sigma) and collect the filtered exosomes by centrifuging at 3500 rpm for 10 min. The obtained filtrate should then be subjected to centrifugation at 150,000 g for 1 h and 30 min. Remove the supernatant and use Dulbecco's phosphate-buffered saline (DPBS, Solarbio) along with 25 mM trehalose (Millipore Sigma) to resuspend the exosomes for further analysis.

The collection of engineered exosomes requires the extraction of exosomes after the transfection of DC2.4 cells. Simply put, DC2.4 cells need to be treated with (1.5 μg/mL) plasmid in each dish, and then the medium should be replaced with complete DMEM medium after 8 h to continue the culture. After 60 h, the cell supernatant is collected, and the exosome extraction process is repeated to obtain engineered exosomes.

After the obtained exosomes were diluted, F-L-R-Exo and L-R-Exo were analyzed by Nanoparticle Tracking Analysis (NTA). The obtained exosomes were immobilized on a copper mesh, stained with tungsten phosphate, and analyzed by transmission electron microscopy (Hitachi HT7800) to observe the particle size and shape changes of the exosomes before and after engineering. In order to verify that the Fc protein is embedded on the surface of exosomes, F-L-R-Exo was incubated with IgG H&L (6 nm Gold)-pre-adsorbed secondary antibody (ab105294, abcam) directly in the refrigerator at 4 °C overnight. After ultracentrifugation at 10,000 g for 30 min, the unbound antibody was removed. Finally, the sample was stained and observed.

2.4. Expression and characterization of the fusion protein

Using CD9 (ab236630, abcam), CD63 (ab134045, abcam), Alix (ab275377, abcam), GM130 (ab52649, abcam), and the DDDDK tag (ab205606, abcam), the primary antibodies were used to perform Western blotting analysis on the engineered exosomes or DC2.4 cells in order to characterize the specific markers of exosomes and the expression of target proteins. After being transfected, DC2.4 cells were incubated with a DDDDK tag antibody, washed twice with PBS, conjugated to a FITC secondary antibody, observed under a confocal laser scanning microscope (CSIM 100/110, SUNNY), or harvested for examination in a flow cytometer (Attune NxT, Invitrogen).

2.5. Exosome content detection

Exosomes were extracted from transfected DC2.4 cells and collected in RIPA or PBS. The concentration or yield of exosomes was determined using NTA. Then, SARS-CoV-2 (2019-nCoV) Spike RBD ELISA Kit was used to detect the RBD proteins contained in the exosomes, based on the corresponding particle count, according to the instructions provided. Finally, the number of RBD proteins carried by each exosome was calculated based on the molecular weight of the fusion protein.

2.6. LNPs self-assembly

Dissolve the lipid components (SM-102, cholesterol, DSPC, DMG-PEG2000) in ethanol to obtain a clear lipid solution. The molar ratio of SM-102, cholesterol, DSPC, and DMG-PEG2000 is 50:38.5:10:1.5. The total concentration of lipids is 10 mM. Prepare 25 mM citrate buffer solution at the pH 4.0, which acts as the aqueous phase. Load the lipid solution into a syringe and the aqueous buffer into another syringe. Connect the syringes to the microfluidic mixing device. Set the total flow rates at 8 ml/min. The flow rate ratio of lipid solution and aqueous phase is 1:3. Collect the LNP dispersion at the outlet of the microfluidic device. The LNPs were eluted twice with phosphate-buffered saline (PBS, pH 7.4) and centrifuged at 4 °C (~3500 rpm) using a 100 kDa MWCO centrifugal filter (Millipore, Burlington, MA). Subsequently, they were eluted and concentrated using PBS solution containing 10 % sucrose. LNPs were eventually filtered through a 0.22 μm filter membrane.

2.7. Stability study of exosomes

Exosomes were collected in DPBS containing 25 mM trehalose, and their morphology, particle size, and RBD protein content were observed under NTA and transmission electron microscopy after being cultured at room temperature for 2 days, room temperature for 2 weeks, and 4 °C for 2 weeks.

2.7.1. The targeting ability of F-L-R-Exo/LNPs following intratracheal injection

F-L-R-Exo/LNPs were labeled with fluorescent dye 1,1-dioctadecyl-3,3,3,3-tetramethylindotricarbocyanine iodide (DiR) (dye concentration, 0.05 mM). After incubation at 37 °C for 2 h, the unbounded dye was

separated using an Exosome Spin Columns (Invitrogen), and removed by centrifugation at10,000 g, 4 °C for 15 min. Then, the resultant DiR-labeled F-L-R-Exo/LNPs were intratracheal injected into the lung at a dose of 10^9 particles per mouse. The IVIS Spectrum Imaging System (PerkinElmer) was used for observation of the fluorescent signal. For ex vivo visualization, the major organs were harvested at any time points, and the DiR fluorescent signal was measured.

2.8. Construction of lung epithelial model

Calu-3 cells (CL-0054; Pricella) were cultured in Minimum Essential Medium (containing NEAA), supplemented with 10 % fetal bovine serum and 1 % penicillin/streptomycin to create a complete medium. Calu-3 cells were changed every other day when they were seeded on Petri dishes. After three passages, the cells were digested with trypsin-EDTA and counted using a cell counter (Countess 3, Invitrogen). The cells were resuspended in complete medium to achieve a cell density of about 2×10^5 cells/mL. Once the cells were full in the transwell membrane, the culture medium in the transwell chamber was discarded, and only the culture medium on the lower side was supplied to initiate air-liquid interface culture. The resistance value was measured every 3 days during the air-liquid culture. After equilibrating in the incubator for 20–30 min, a resistance meter was connected, an electrode tip was inserted into the transwell chamber, and the measurement and reading were started. Three different positions were measured in each well, the average value was calculated, and the value of the blank well was subtracted. The transwell membrane surface area (1.12 cm2) is used to calculate the trans-epithelium electrical resistance (TEER), which is the resistance across the epithelial layer. When the TEER value of Calu-3 cells cultured with ALI reached 500–800 Ω•cm2, the tight junction epithelial model was formed. The extracted F-L-R-Exo and L-R-Exo were incubated with FcRn antibody (ab228975, abcam) in the transwell model for 24 h, and NTA was used to detect the number of particles containing fluorescence in the lower side of the transwell medium at a 488 nm wavelength.

2.9. Internalization of exosomes by DC2.4 cells

Commercial RBD protein (40592-V08B, SinoBiological) was labeled with FITC, and engineered exosomes' RBD protein was labeled with antibody. DC2.4 cells were cultured for another 4h, and then washed with PBS twice. The cells were collected and analyzed by flow cytometry.

2.10. Biosafety and ethics

All studies complied with the requirements of the Institutional Animal Care and Use Committee (IACUC-DWZX-2023-516). Female BALB/c mice or K18-hAEC2 mice, aged 6–8 weeks, were obtained from Beijing Vital River Laboratory Animal Technology Co. Ltd. L-R-Exo, F-L-R-Exo treatments (10^{10} per kg of mouse weight) and RBD-Lipo treatments (1.26×10^{10} per kg of mouse weight) were given in two doses, once a week for 2 weeks, via nebulization or IV injection. All animal studies were conducted under ethical codes and approved by the local ethics committee.

2.11. Enzyme-linked immunosorbent assay

Commercial RBD proteins were diluted in coating solution (0.1 M, pH 9.6) and coated in 96-well EIA/RIA plates (Coning) overnight at 4 °C. They were then washed three times with PBST (0.05 % Tween-20) and blocked with 150 μL of blocking solution (2 % BSA, PBST) added to each well for 2 h. Then, 300 μL of PBST wash solution was added to each well of the 96-well plate for three washes. Serum/bronchoalveolar lavage fluid (BALF) samples were diluted with 0.1 % BSA (PBST) in the first well (1/300), and then diluted 3 times further, with 100 μL per well, and incubated at 37 °C for 1 h. After washing, the samples were assayed for 1 h with HRP-conjugated goat anti-mouse IgG antibody (1:2000) or HRP-conjugated goat anti-mouse IgA antibody (1:5000). For the mouse experiment, IgG subclasses were determined for 1 h using HRP-conjugated goat anti-mouse IgG2a monoclonal antibody (ab97245, abcam) and HRP-conjugated goat anti-mouse IgG1 monoclonal antibody (ab97240, abcam), followed by five washes of the plate with PBST. TMB substrate (Solarbio) was used for color development, which was then terminated by adding 50 μL of termination solution. Absorbance was read at 450 nm using a microplate reader within 10 min. An OD value higher than twice the OD value of a negative serum was considered positive, and the maximum dilution was the titer value of the antigen-specific antibody in the serum of that sample.

2.11.1. Cytokine measurement in splenocytes and pneumonocytes

Each vaccinated mouse was challenged with RBD peptide pools (4 μg/mL/peptide) and placed into Elispot wells (Splenocytes 10^6/well, Lung cell 5×10^5/well) (MSIPS4W10, Millipore) that were coated with anti-mouse IFN-γ capture antibody (5179021, biolegend). After 22 h of culture, the supernatant was discarded, then the cells were lysed twice with precooled pure water, and the cells were incubated for 2 h at room temperature with biotinylated IFN-γ detection antibody (505704, biolegend) in each well. After washing, the incubation was continued with HRP Avidin (405103, biolegend) for 1h. Finally, TMB substrate was added for color development for 30min, and the color reaction was terminated using a clear rinse board. The plates were then placed in a dry environment in the dark until completely dry. The number of spots formed was analyzed and counted by a plate reading instrument (ImmunoSpot® Analyzers).

2.11.2. Immune activation of pneumocytes

Splenocytes were harvested on day 21 post-inoculation and seeded into 96-well plates at a density of 10^6 cells/well. The splenocytes were stimulated with SARS-CoV-2-S RBD (PP002-A, SinoBiological) (5 μg/mL) for 1h in a cell incubator. Then Brefeldin A (1 μg/mL) was added to the splenocytes for another 5 h, and the cells were collected. CD3-PE (100205, biolegend), CD4-FITC (100405, biolegend), and CD8a-Pacific Blue (506715, biolegend) were used for phenotypic staining. For intracellular factor staining, IFN-γ (505809, biolegend), TNF-α (506307, biolegend), IL-4 (504105, biolegend), and IL-2 (503809, biolegend) were used. After 1 h of intracellular factor staining incubation, the cells were washed and examined by flow cytometry (Attune NxT, Invitrogen).

2.12. SARS-CoV-2 D614G pseudovirus challenge

For in vitro imaging experiments, mice were immunized with F-L-R-Exo and L-R-Exo for two weeks. On day 21, 40 μL of SARS-CoV-2 (D614G)-GFP-Luc pseudovirus (XCV03, Novoprotein) was delivered to the lungs of each mouse. The lungs of the mice were injected with 100 μL of potassium fluorescein solution, and 2 min later, the lungs were removed. The experimental data were quantitatively analyzed using a mouse in vivo imager (IVIS Spectrum, PerkinElmer) and Living Image software.

2.13. Pseudovirus microneutralization assay

After immunization, 150 μL of blood was collected from the inner canthus vein of the mouse. The blood samples were left at room temperature for 4h, centrifuged at 5000 rpm for 10min, and inactivated with complement at 56 °C for 30min. The Hela-hACE2 cells were resuscitated and adjusted to the desired state. The cells were screened with G418 (ant-gn-1, InvivoGen), HygromycinB Gold (ant-hg-1, InvivoGen), and cultured for 3 days, with the solution being changed every other day. The diluted serum sample was added to a 96-well plate, and 10 μL of SARS-CoV-2 D614G was added to each well. The plate was then placed in an incubator at 37 °C for 1h. After that, adjusted Hela-hACE2 cells

(5.0×10^4/well) were added to the virus-serum complexes, and the cells were incubated for 48 h. After incubation, the cell supernatant was removed, the cells were lysed, and the luciferase signal was detected using the Bright-Glo firefly luciferase kit (Promega). The neutralization rate was calculated, and the EC50 titer was determined.

2.14. Statistical analysis

All quantitative experiments were repeated three times independently, and data are presented as mean ± SD. The unpaired nonparametric Mann-Whitney test was used to compare the values between the two groups. A one-way ANOVA was used to compare the differences between the two groups. GraphPad Prism was used for all statistical analyses. P value less than 0.05 is considered to indicate statistical significance.

3. Results

3.1. Preparation and characterization of exosomes carrying Fc-Lamp2b-RBD

To express the fusion protein on exosomes, we fused the mammalian-optimized Fc sequence (GenBank: KY053479.1), Lamp2b sequence (GenBank: AK304405.1), and RBD sequence (R319-F541; GenBank: OP912878.1) in a plasmid using pcDNA3.1 as a vector and named it F-L-R (Fig. 2a). Lamp2b-RBD (L-R) was used as a comparison. The intracellular expression of F-L-R and L-R was confirmed by immunofluorescence, showing that the target proteins were localized on the cell membrane of DC2.4 cells (Fig. 2b). Flow cytometry and reverse transcription quantitative polymerase chain reaction (RT-qPCR) were used to further confirm the expression of the target proteins, as 65 ± 5 % of cells showed positive staining (Fig. 2c and Supplementary Fig. 1). Exosomes secreted by DC2.4 cells were obtained through gradient centrifugation and ultracentrifugation. The presence of positive markers CD9, CD63, Alix, and the absence of the negative marker GM130 in the exosomes were confirmed (Fig. 2d) Transmission electron microscopy (TEM) showed the uniformity of the harvested exosomes, with a typical cup-shaped appearance (Fig. 2e). The size of the exosomes was determined using nanoparticle tracking analysis (NTA), and the average particle size of the exosomes was found to be approximately 100–120 nm (Fig. 2f). To confirm the successful loading of F-L-R and L-R, we first labeled F-L-R with gold nanoparticles and characterized the exosomes by TEM. Results showed that Fc fragments were successfully detected on the outer membrane of exosomes, with 3 Fc fragments labeled on each exosome (Fig. 2g). Additionally, NTA results showed a slight increase in the particle size of F-L-R-Exo (Fig. 2h). Furthermore, Western blot experiments using lysates of F-L-R-Exo and L-R-Exo demonstrated the presence of specific bands with predicted molecular weights (Fig. 2i). These findings provide evidence for the successful loading of fusion proteins onto exosomes. To quantify the incorporated RBD antigens in the exosomes, an enzyme-linked immunosorbent assay (ELISA) was performed using intact exosomes or their lysate. Almost no RBD could be detected in intact exosomes, suggesting that the antigens may be incorporated into the lumen of exosomes with undetectable leakage. After lysis, RBD was quantified to be 332 ± 15 pg per 108 exosomes (Fig. 2j). The exosomes could be effectively preserved for at least 2 weeks at room temperature without observable changes in morphology (Fig. 2k and Supplementary Fig. 2), particle size, particle concentration, or RBD protein content (Fig. 2l), indicating good stability of the exosomes.

3.2. The biodistribution of exosomes in lung is better than that of LNPs

Lipid nanoparticles (LNPs), as the only approved mRNA vaccine delivery materials by the U.S. Food and Drug Administration (FDA), showed their superiority in combating the pandemic of COVID-19 and hold exceptional promise for additional therapeutic strategies. Therefore, LNPs were used as a counterpart to study the retention and distribution of exosomes in mouse lungs [43]. To achieve this, LNPs were prepared by a microfluidic chip as previously described (Supplementary Fig. 3), and the particle concentrations of LNPs and F-L-R-Exo were equalized (1.0E+10 particles/mL) before intratracheal administration (Fig. 3a). In vivo imaging demonstrated that both LNPs and exosomes reached the lungs after 2 h. However, the distribution and retention of exosomes in the lung were significantly higher than that of LNPs after 24 h (Supplementary Fig. 4). Meanwhile, F-L-R-Exo exhibited substantial retention in the lung after 24 h, whereas LNPs decreased rapidly after 24 h (Fig. 3c). To further quantify the disparity between LNPs and exosomes, the lungs of the mice were removed after 4 h and 24 h after administration for immunofluorescence analysis (Fig. 3d). The results showed that compared to exosomes, more LNPs were trapped in the trachea at both 4 h and 24 h (Fig. 3e). The distribution of exosomes in the bronchioles was found to be highest at 24 h after administration (Fig. 3f). By Fc decoration, exosomes were supposed to cross the lung epithelial cells and penetrate to the lung parenchyma efficiently. As expected, exosomes showed a significantly higher fluorescence signal in lung parenchyma at both 4h and 24h (Fig. 3g).

To confirm whether F-L-R-Exo pass through lung epithelial cells mainly relies on FcRn-mediated transcytosis, we established an in vitro model using Calu-3 cells that express FcRn when polarized [44]. In the control group, FcRn was blocked using antibodies and the experiment was conducted in a transwell chamber. Following incubation, NTA was used to measure the number of exosome particles in the lower chamber. The results revealed that F-L-R-Exo exhibited a significantly higher retention of particles in the lower compartment compared to the L-R-Exo and anti-FcRn-Exo groups (Fig. 3h), indicating the dominating role of FcRn during the process of exosomes passing through the lung epithelial barrier.

To determine whether exosomes could be taken up by DC cells after penetrating the lung parenchyma, high levels of CD11c + antigen presenting cells, which were induced by F-L-R-Exo, were detected in BALB/c mice 21 days after immunization (Fig. 3i). Flow cytometry was employed to quantify the uptake of F-L-R-Exo, and the commercial RBD protein was used as a control. Both F-L-R-Exo and the commercial RBD protein were incubated in DC2.4 cells at an equivalent RBD concentration. The results revealed that the cells exhibited minimal or no uptake of commercial RBD proteins. In contrast, F-L-R-Exo exhibited remarkably higher uptake ability (Fig. 3j). In addition, RBD protein could not only activate DC2.4 cells in vitro (Supplementary Fig. 5), but the F-L-R-Exo, which was extracted, also carried costimulatory cytokines CD80 and CD86, speculated to activate T cells with high intensity and induce immune responses (Supplementary Fig. 6).

3.3. F-L-R-exo effectively induced mucosal immune response

BALB/c mice were vaccinated twice a week with placebo (PBS), L-R-Exo (intratracheally), F-L-R-Exo (intratracheally), and once with F-L-R-Exo (intramuscularly, IM) (Fig. 4a). RBD-specific IgG antibody titers were measured at Week 1 and Week 3. Although no significant difference was observed between the groups at Week 1, the antibody titers in the F-L-R-Exo group were generally 3 to 9 times higher than those in the F-L-R-Exo (IM) group (Fig. 4b). On day 21 after inoculation, F-L-R-Exo induced the highest levels of RBD-specific IgG antibodies, with a significant difference in titers compared to the L-R-Exo and F-L-R-Exo (IM) groups (Fig. 4c). Then, the subclass spectrum of RBD-specific antibody in serum was evaluated and found that mice treated with F-L-R-Exo showed higher IgG2a antibody titers, while mice treated with F-L-R-Exo (IM) had higher IgG1 antibody titers. These results suggest that intratracheal delivery induced a Th1-type immune response in mice, with a ratio of IgG2a/IgG1 > 1. Additionally, the RBD-specific IgG and sIgA antibody titers in the bronchoalveolar lavage fluid were detected (Fig. 4e and f). The results revealed that the F-L-R-Exo (IM) group had

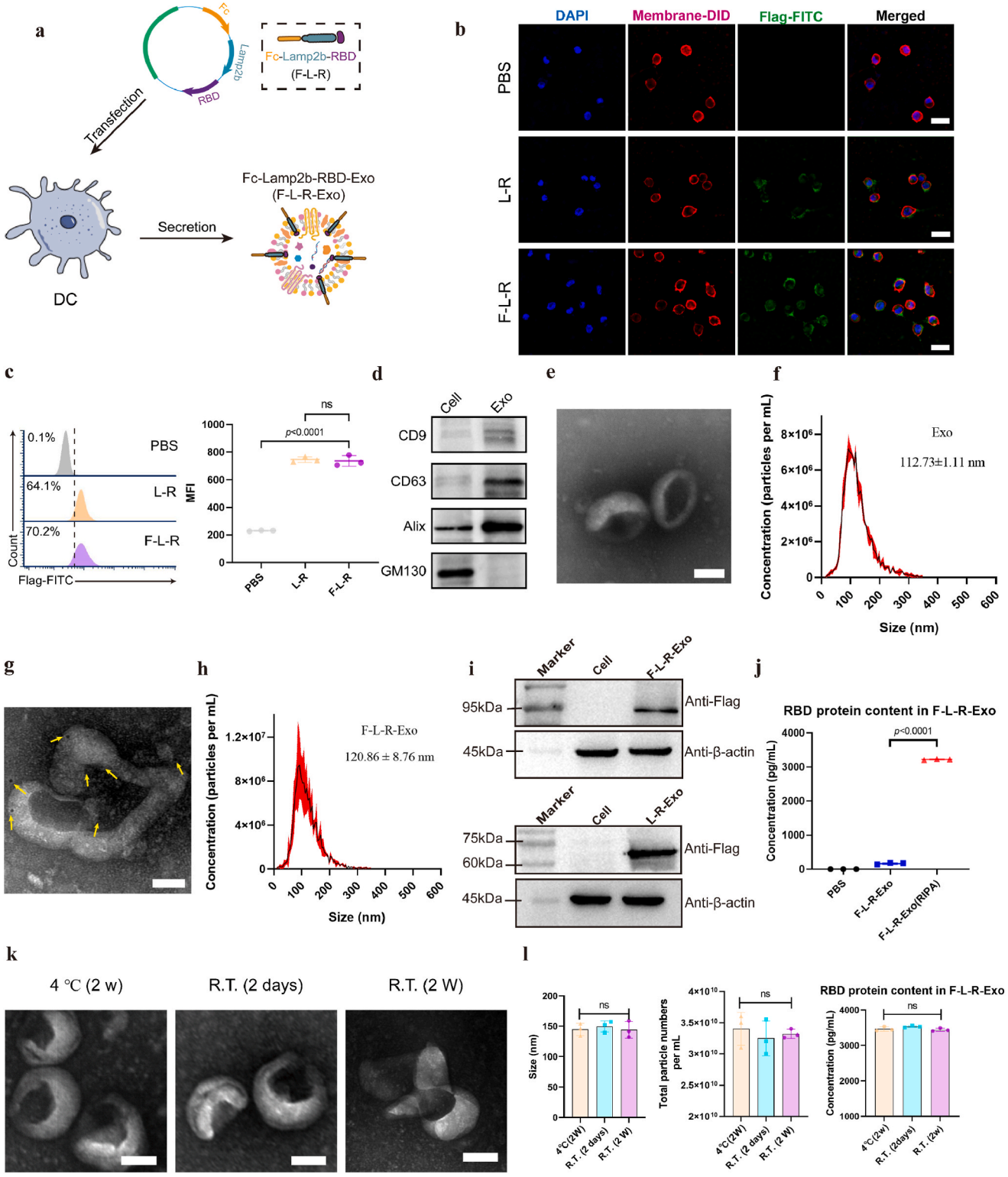

Fig. 2. Characterization of the fusion proteins. **a,** a schematic illustration of Fc-Lamp2b-RBD loaded on exosomes after transfection of plasmids to DC2.4 cells. **b,** Representative immunostaining of DC2.4 cells for DAPI (blue) and membrane (red) or Flag (green). Scale bar, 10 μm **c,** Cellular expression of F-L-R and L-R (left) and the mean fluorescence intensity (MFI, right), verified by flow cytometry. ($n = 3$) **d,** Immunoblotting of CD9, CD63, Alix, and GM130 of lysed cells and Exo. **e,** TEM image of DC-Exo. Scale bar, 100 nm. **f,** DC-Exo concentration and particle size was detected by NTA, and the original concentration was diluted by 1:1000, ($n = 3$). **g,** TEM image of F-L-R-Exo. RBD protein signals were found using antibodies labeled with gold nanoparticles with a diameter of 6 nm. Scale bar, 100 nm. **h,** F-L-R-Exo concentration and particle size was detected by NTA, and the original concentration was diluted by 1:1000. ($n = 3$) **i,** Immunoblot using lysis of cells, F-L-R-Exo, and L-R-Exo. Anti-flag antibody was used for characterization. **j,** The RBD protein concentration of intact exosomes and their lysis was detected by ELISA. ($n = 3$) **k,** TEM images of F-L-R-Exo under different storage conditions. Scale bars, 50 nm **l,** The size and the particle and RBD protein content concentration of F-L-R-Exo under different storage conditions. ($n = 3$) Experiments were performed three times (b–i). Data in c, f, h, j, i are represented as mean ± SD. ns, not significant. All replication is biological.

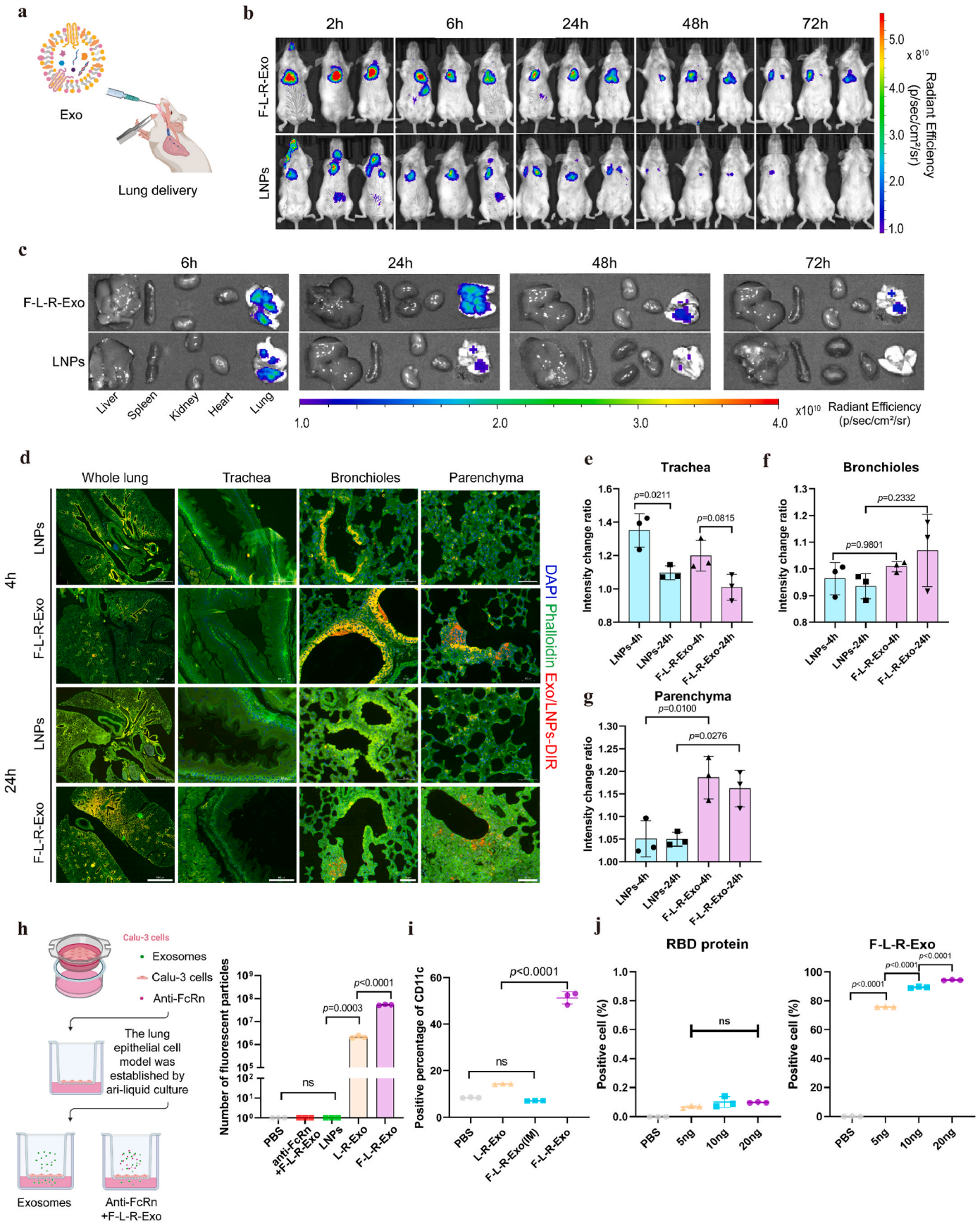

(caption on next page)

Fig. 3. Distribution and uptake of engineered exosomes in the lungs. **a.** Exosomes/LNPs were administered intratracheally to monitor lung tissue distribution over time in BALB/c mice ($n = 3$). **b**, Comparison of biodistribution among LNPs, L-R-Exo and F-L-R-Exo. BALB/c mice were delivered DIR-labeled LNPs, L-R-Exo, and F-L-R-Exo to the lungs, and were imaged in vivo at 4, 6, 24, 48 and72 h **c,** Ex vivo imaging of mouse lung tissue captured at various time intervals, ($n = 3$). **d,** Immunostaining of DAPI (blue), phalloidin (green), and exosomes (red) or LNPs (red) in whole lung, trachea, bronchus, and parenchyma sections. The whole lung. Scale bar, 2000 μm. These images were obtained under × 10 magnification. The trachea. Scale bar, 100 μm. The bronchiole and lung parenchyma. Scale bar, 50 μm. **e-g,** Each dot represents the ratio of exosome/LNPs (red) to cytoskeletal (green) fluorescence at a site, ($n = 3$). **h**, F-L-R-Exo and L-R-Exo were labeled with DIO, and the concentration of nanoparticles in each group in the lower chamber was detected on NTA with an absorption wavelength of 500 nm, ($n = 3$). **i**, The lung tissue of euthanized BALB/c mice was removed on day 21, and CD11c was used to label the antigen-presenting cells in the lungs of the mice, ($n = 3$) **j**, The positive fluorescence rate of DC2.4 cells was determined after incubation with FITC-labeled F-L-R-Exo (right) or commercial RBD protein (left) for 6 h. All replicates are independent.

negligible levels of RBD-specific sIgA antibody titers, whereas the F-L-R-Exo group exhibited a 10-fold higher sIgA antibody titer compared to the L-R-Exo group. The results of the study showed that intratracheal administration successfully induced a mucosal immune response. Furthermore, the findings suggested that exosomes modified with Fc were more effective in eliciting this response.

Naive B cells were stimulated with antigens and activated with the assistance of T cells in peripheral immune organs. Subsequently, they entered a proliferative state to form Germinal Center B cells (GC B). The induction of high-quality durable B cells relies on the GC response [45]. We collected whole lung cells from mice after 2 weeks of immunization for GC B cell analysis. Results showed that F-L-R-Exo immunization led to a significant increase of GC B cells (Supplementary Fig. 7), while the F-L-R-Exo (IM) group did not show a significant difference compared to the L-R-Exo group and the PBS group (Fig. 4g). Apart from B cell responses, T cell responses, especially tissue-resident memory T cells, also play a vital role in clearing virus at the site of infection [46]. Hence, lung Trm response was evaluated at 21 days, and the results showed that F-L-R-Exo elicited a potent Trm response (Fig. 4h) (Supplementary Fig. 8). Such results were further observed in lung tissue, when F-L-R-Exo was immunized intratracheally, but not intramuscularly, inducing the formation of bronchial associated lymphoid tissue (iBALT) (Supplementary Fig. 9) [32].

3.4. F-L-R-exo induced a strong Th1-biased immune response

Strong immune responses were induced by F-L-R-Exo in the lungs of BALB/c mice. FcRn is expressed not only on epithelial cells but also on the surfaces of many lymphocytes and actively participates in antigen presentation pathways leading to immune cell activation, proliferation, and T cell interactions [47]. Thus, FcRn may have the potential to amplify the immune response, leading to a higher level of cytokines like IFN-γ [48].

To assess T cell responses induced by F-L-R-Exo in mice, splenocytes and pneumonocytes were stimulated with an RBD-peptide pool respectively, and the RBD-specific T cells were quantified using an enzyme-linked immunospot assay (Elispot). Following stimulation of lung cells with the polypeptide pool, a robust Th1-polarized T cell response was elicited upon immunization, demonstrated by increased levels of RBD-specific IFN-γ-producing T cells in both the lung and spleen (Fig. 5a). Notably, F-L-R-Exo administered intratracheally induced approximately 500 spot-forming units per 10^6 pneumonocytes, which was significantly higher compared to the other groups. Interestingly, higher levels of IFN-γ were observed in splenocytes of the IM group compared with the intratracheal instillation group, but with no significant difference (Fig. 5b). To investigate the reason, splenocytes of BALB/c mice were collected 4 weeks after immunization, and the cytokines released by T cells after stimulation with the RBD peptide pool were detected by intracellular cytokine staining (ICS) assay. F-L-R-Exo significantly increased the release of TH1 type cytokines in RBD-specific CD8+T cells, such as IFN-γ, IL-2, TNF-α, and a small amount of IL-4. When F-L-R-Exo was administered to the lung, it also caused CD8+T cells to be biased towards Th1 immunity (Fig. 5c, d, e, f). On the other hand, intramuscular administration of F-L-R-Exo led to higher levels of IFN-γ and IL-4 in $CD4^+$ T cells (Fig. 5g, h, i, j). These results suggest that F-L-R-Exo may require a sufficient number of $CD4^+$ T helper cells to induce a high-quality immune response by intramuscular injection. Ultimately, these results are consistent with the IgG2a/IgG1 ratio in vaccinated mice. Thus, intratracheally administered F-L-R-Exo could induce a Th1-biased immune response.

Safety assessments were performed on BALB/c mice on day 21 of immunization. There were no obvious pathological changes in the pathological sections of the main organs, and the body weight of mice in all groups did not change significantly during the treatment process (Supplementary Fig. 10). The systemic toxicity of different vaccines was evaluated by measuring biochemical markers. The results showed that all serum biochemistry parameters remained at normal levels (Supplementary Fig. 11).

3.5. F-L-R-exo can achieve efficient clearance of pseudoviruses

BALB/c mice exhibited good immune responses in immunological experiments. To further assess the immune effects in different mouse strains, K18-hACE2 transgenic mice were immunized using the same procedure (Fig. 6a). After three weeks of immunization, a higher level of RBD-specific IgG antibody titers in serum (Supplementary Fig. 12a) and a higher level of RBD-specific sIgA titers in BALF were again observed in the F-L-R-Exo group (Supplementary Fig. 12b).

On day 21 post-immunization, K18-hACE2 mice were infected with SARS-CoV-2 D614G pseudovirus through intratracheal administration. Two days after infection, luciferase activity and green fluorescent protein (GFP) expression were detected. Ex vivo lung imaging results revealed that mice in the PBS group had a large area of pseudovirus infection and the highest fluorescence intensity. Both L-R-Exo and F-L-R-Exo (IM) groups showed a high level of viral infection in the lungs, though lower than in the PBS group. However, the F-L-R-Exo group exhibited extremely low levels of virus infection, indicating a good protective effect of the vaccine (Fig. 6b). Immunofluorescence results of the lungs again showed that the SARS-CoV-2 D614G pseudovirus was less distributed in the trachea in the F-L-R-Exo and L-R-Exo groups compared to the F-L-R-Exo (IM)-treated group. Additionally, the GFP signal in the lung parenchyma was significantly reduced in the F-L-R-Exo group (Fig. 6c–e). These results proved that F-L-R-Exo accelerated the clearance of SARS-CoV-2 D614G pseudovirus in the lung parenchyma. To further investigate the clearance efficiency, lung cells were collected and the GFP fluorescence was measured using flow cytometry. The results were consistent with the ex vivo imaging of lung tissues, showing a significantly higher virus clearance efficiency in the F-L-R-Exo group (Fig. 6f). Apart from mucosal immunity, a pseudovirus neutralization assay was performed to assess the neutralizing capacity of antibodies elicited by the vaccines. Neutralizing antibodies were detected in the sera of each vaccinated group. Among these groups, F-L-R-Exo exhibited the highest neutralizing antibody titer, while the L-R-Exo and F-L-R-Exo (IM) groups had equal levels of neutralizing antibodies. These findings suggest that F-L-R-Exo was able to elicit both mucosal and humoral immune responses against the SARS-CoV-2 D614G pseudovirus.

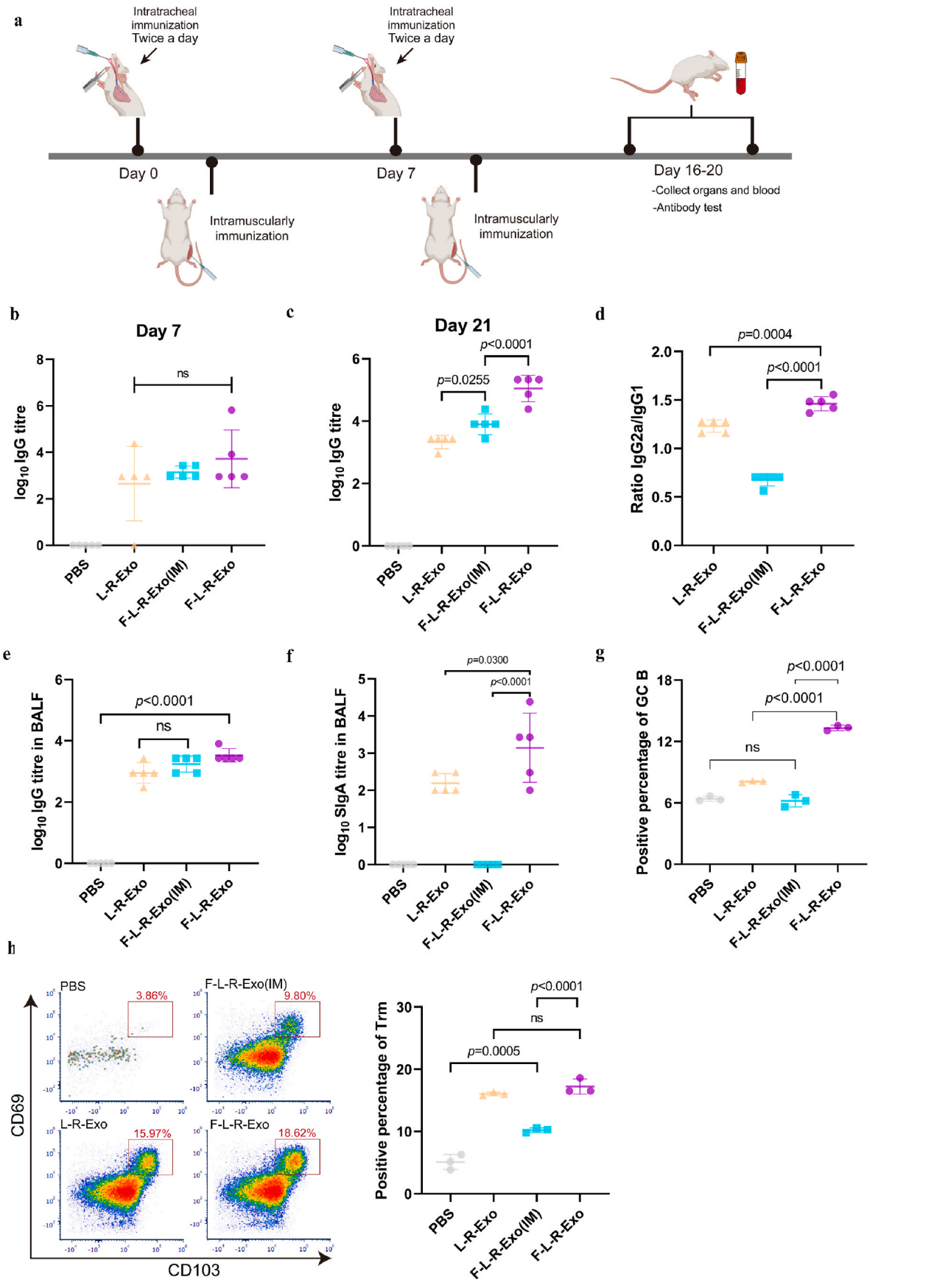

(caption on next page)

Fig. 4. The engineered exosome vaccine could induce RBD-specific immune responses in mice. **a,** A schematic illustration of animal immunization. Barb/c mice were immunized for two weeks to assess the immunogenicity and protective effects of the vaccine. Barb/c mice were inoculated with either F-L-R-Exo or L-R-Exo at Week 0 and Week 1. RBD-specific IgG titers were measured by ELISA at weeks 1 and 3, ($n = 5$). **b,c** RBD protein specific IgG titers were detected in mouse serum by ELISA on days 7 and 21, ($n = 5$). **d,** The ratio of RBD-specific IgG2a to IgG1 antibodies generated in serum was measured at week 3, ($n = 3$). **e,f,** RBD-specific IgG antibody titers (**f**) and SIgA antibody titers (**g**) in BALF measured by ELISA, ($n = 5$). **g,** On day 21, BALB/c mice were sacrificed, and lung tissues were removed for GC reaction detection using FAS^+GL7^+ and $CD19^+$, ($n = 3$). **h,** BALB/c mice were euthanized on day 21, and the lung tissues were taken out, and $CD103^+CD69^+CD45^-$ and $CD3^+$ were detected for Trm cells, ($n = 3$). All replicates were biological, and the flow chart in **a** was created with BioRender.

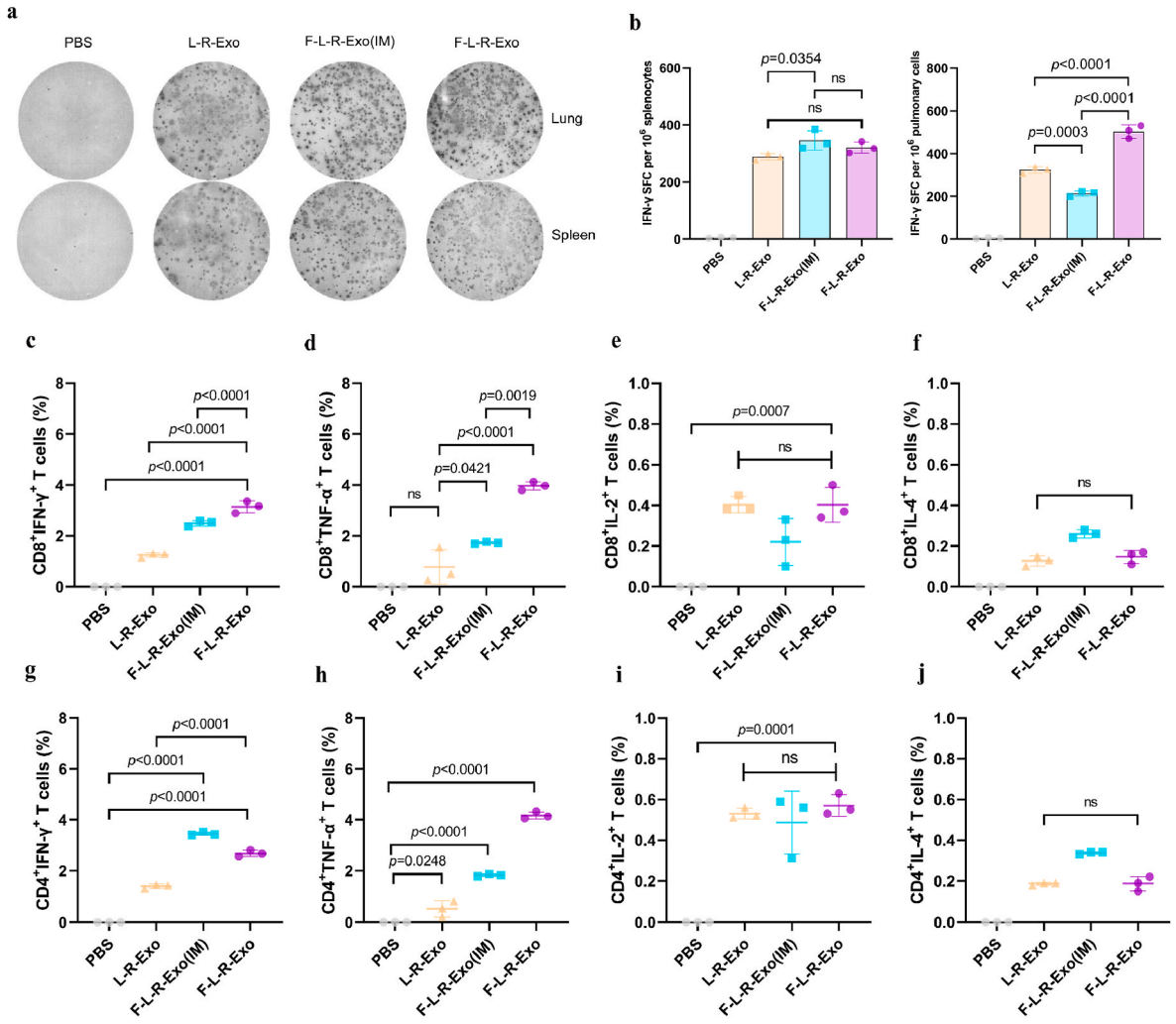

Fig. 5. F-L-R-Exo induced TH1-type cytokine immune responses in mice. **a,** On day 21 after BALB/c mice were vaccinated, the lungs and spleen of the mice were removed and stimulated with an RBD polypeptide pool, and IFN-γ was released on 96-well plates with 1×10^6 spleen cells or lung cells in each well. The spleen and lung tissue from mice in each group was obtained from those that had received the corresponding immunizations. **b,** IFN-γ splenocytes and lung cells shown as spot forming cells (SFC) per 10^6 cells, ($n = 3$). **c-f,** $IFN\text{-}\gamma^+$, $TNF\text{-}\alpha^+$, $IL\text{-}2^+$ or $IL\text{-}4^+$ $CD8^+$ T cells. **g-j,** $IFN\text{-}\gamma^+$, $TNF\text{-}\alpha^+$, $IL\text{-}2^+$ or $IL\text{-}4^+$ $CD4^+$ T cells. **c-j,** On day 21 after vaccination, cytokines produced by splenocytes stimulated with the RBD peptide pool were analyzed by intracellular factor assays. All replicates were biological.

4. Discussion

Through our evaluation of the immune effects induced by various modified exosomes, we gained a profound understanding of the influence of Fc protein chimerism in exosomes on intratracheal administration, as well as the variations in immune responses resulting from different vaccination approaches. Regardless of the treatment strategy for COVID-19, effective vaccination remains critical. Exosome-based engineered vaccines demonstrate clinical potential in eliciting antibody responses that can prevent and neutralize SARS-CoV-2.

In this study, we utilized DC-derived exosomes for lymphatic homing and immune activation. When administered via the trachea, F-L-R-Exo elicited a robust cellular immune response. F-L-R-Exo demonstrated remarkable stability and a high antigen-bearing capacity. Additionally, it exhibited prolonged retention time and good distribution ability in the lung. F-L-R-Exo proved to be a more advanced mucosal delivery system compared to commercial LNPs. In the immunization experiment of BALB/c mice, F-L-R-Exo demonstrated effective induction of mucosal and systemic immune responses. However, L-R-Exo and F-L-R-Exo (IM) exhibited weaker induction effects. F-L-R-Exo was administered intratracheally to immunize mice. This method allows F-L-R-Exo to penetrate the FcRn lung epithelial cell receptor, thereby activating the mucosal immune system and inducing the production of high-titer IgG antibodies. This process can also trigger the production of high-titer IgA antibodies, activate additional antigen-presenting cells, and stimulate tissue-resident memory T cells, thereby inducing a systemic immune response. Notably, in BALB/c mice, the injection of the F-L-R-Exo vaccine into the lungs induced a Th1-biased immune response, as evidenced

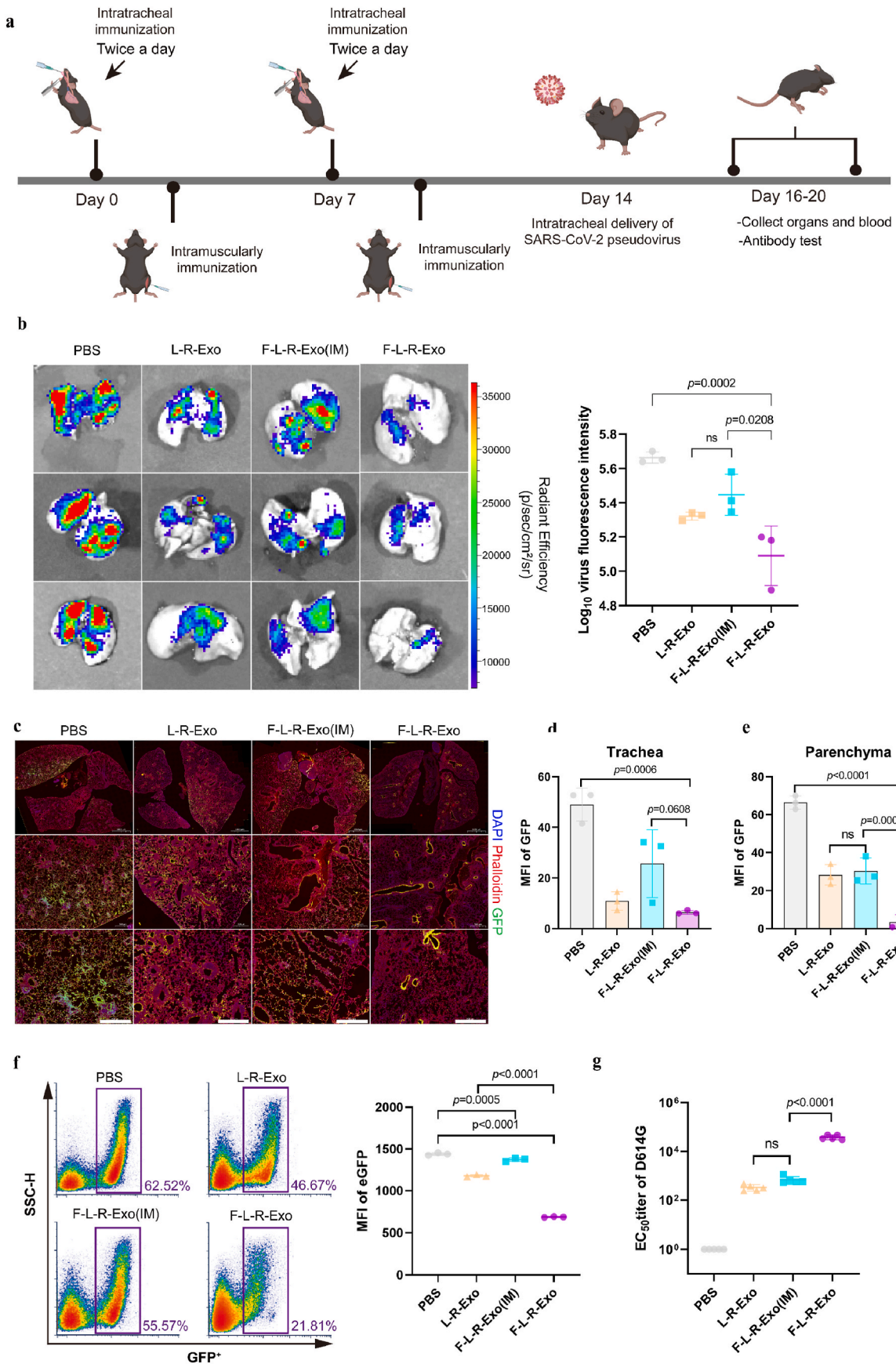

(caption on next page)

Fig. 6. The SARS-CoV-2 D614G pseudovirus was effectively neutralized in immunized mice in each group. **a,** A schematic illustration of animal immunization. K18-hAEC2 mice were immunized for two weeks to evaluate the immunogenicity and protective effect of the vaccine. K18-hAEC2 mice were inoculated with F-L-R-Exo or L-R-Exo at week 0 and 1. RBD-specific IgG titers were measured by ELISA at weeks 1 and 3, ($n = 5$). **b,** The lungs of mice in each group were challenged by SARS-CoV-2 D614G pseudovirus at the third week after immunization. In the in vitro imaging of lung tissue on the second day after the challenge, the pseudovirus produced luciferase after expression and delivered luciferase substrate to the lungs before killing the mice. Each point in the right figure represented the lung fluorescence intensity of a mouse, ($n = 3$). **c,** Immunostaining imaging of whole lung (upper row), trachea/bronchiole (middle row), and parenchyma (lower row) of mice inoculated with different vaccines with DAPI (blue), phalloidin (red), and SARS-CoV-2 D614G pseudovirus (green). Scale bar, 500 μm, ($n = 3$). **d,e** Quantification of the mean fluorescence intensity of the trachea or lung parenchyma, with each point representing a part of lung tissue data. Scale bar, 500 μm, ($n = 3$). **f,** Overlapping histograms of GFP positive expression rates in lung cells of each group of mice were verified by flow cytometry, and the mean fluorescence intensity after quantification is shown on the right. **g**, Neutralizing antibodies titers are shown as EC_{50} values, calculated by Reed-Muench method, ($n = 5$). All data were mean ± standard deviation. One-way ANOVA was used for statistical analysis and the flow chart in **a** was created with BioRender.

by increased secretion of related factors in $CD4^+$ and $CD8^+$ T cells. In the K18-hACE2 mouse model, the F-L-R-Exo group, administered via intratracheal injection, exhibited the lowest degree of infection by the SARS-CoV-2 D614G pseudovirus. Neutralizing antibodies were detected in the serum of each vaccination group, with F-L-R-Exo demonstrating the highest neutralizing antibody titer, while the neutralizing antibody levels of the L-R-Exo and F-L-R-Exo (IM) groups were the same.

Dendritic cell-derived exosomes, as naturally occurring biologically active materials, have garnered significant attention in recent years due to their high degree of biocompatibility and safety. These exosomes exhibit low immunogenicity, allowing for natural interaction with target cells without the need for exogenous substances, thus reducing the risk of immune rejection, which is crucial for clinical treatments [49]. In clinical trials, dendritic cell-derived exosomes have also demonstrated good safety, such as in the use of Exo vaccines for advanced malignancies, which have been proven safe and effective, providing strong support for clinical applications [50,51]. Taken together, dendritic cell-derived exosomes have excellent qualities, high biocompatibility, and immune function, making them an ideal scalable drug delivery platform.

Respiratory mucosal immune response plays a crucial role in the initial invasion of pathogens [52,53]. The restricted innate immune responses in infected lung tissue may contribute to the uncontrolled late lung injury observed in late-stage COVID-19 [54]. Currently, some studies have begun using freeze-drying technology to store and transport exosomes, ensuring that their morphology and function remain intact [55,56]. While most vaccines are still administered through injections, there is a growing understanding of respiratory tract infection viruses and the importance of tissue-resident memory T cells in the mucosal site of the respiratory tract. These cells can quickly encounter antigens and respond, making mucosal vaccines a potentially more acceptable method. Lung vaccination can be administered through inhalation, which can indirectly enhance vaccination compliance.

Data availability

The data sets used for the current study are available from the corresponding author upon reasonable request.

Ethics approval and consent to participate

Biosafety and ethics: All studies complied with the requirements of the Institutional Animal Care and Use Committee (IACUC-DWZX-2023-516). Female BALB/c mice or K18-hAEC2 mice, aged 6–8 weeks, were obtained from Beijing Vital River Laboratory Animal Technology Co. Ltd, L-R-Exo、F-L-R-Exo treatments (1010 per kg of mouse weight) and RBD-Lipo treatments (1.26 × 1010 per kg of mouse weight) were given in two doses once a week for 2 weeks via nebulization or IV injection. All animal studies were conducted under ethical codes and approved by the local ethics committee.

CRediT authorship contribution statement

Fan Meng: Writing – review & editing, Writing – original draft, Visualization, Validation, Supervision, Software, Resources, Project administration, Methodology, Investigation, Formal analysis, Data curation, Conceptualization. **Haonan Xing:** Writing – review & editing, Writing – original draft, Validation, Resources, Methodology, Investigation, Funding acquisition, Data curation, Conceptualization. **Jingru Li:** Writing – review & editing, Visualization, Validation, Software, Formal analysis, Data curation, Conceptualization. **Yingqi Liu:** Writing – review & editing, Visualization, Validation, Methodology, Data curation, Conceptualization. **Li Tang:** Writing – review & editing, Visualization, Supervision, Data curation, Conceptualization. **Zehong Chen:** Validation, Supervision, Data curation, Conceptualization. **Xiran Jia:** Visualization, Validation, Data curation, Conceptualization. **Zenglin Yin:** Visualization, Validation, Data curation, Conceptualization. **Jing Yi:** Visualization, Validation, Data curation, Conceptualization. **Mei Lu:** Writing – review & editing, Visualization, Validation, Resources, Funding acquisition, Conceptualization. **Xiuli Gao:** Writing – review & editing, Visualization, Validation, Resources, Formal analysis. **Aiping Zheng:** Writing – review & editing, Supervision, Resources, Project administration, Methodology, Funding acquisition, Conceptualization.

Declaration of competing interest

A.Z. from the Institute of Pharmacology and Toxicology, Academy of Military Medical Sciences. A patent application entitled "Recombinant plasmid Fc-Lamp2b-RBD and its preparation method and application thereof" was filed. All the other authors declare no conflicts of interest.

Acknowledgements

We appreciate all the laboratory members for their cooperation in this work. This work was supported by the National Key R&D Program of China (2023YFC2605000), National Natural Science Foundation of China (32371440, 32101157, 82104105, 81573357). China Postdoctoral Science Foundation (2021M693966).

Appendix A. Supplementary data

Supplementary data to this article can be found online at https://doi.org/10.1016/j.bioactmat.2024.08.015.

References

[1] G.G. Miao, Z.Q. Chen, H.S. Cao, W.H. Wu, X. Chu, H.Y. Liu, L.Y. Zhang, H.F. Zhu, H.Z. Cai, X.L. Lu, J.F. Shi, Y. Liu, T.T. Feng, From Immunogen to COVID-19 vaccines: prospects for the post-pandemic era, Biomed. Pharmacother. 158 (2023) 114208.

[2] H. Morrison, S. Jackson, H. McShane, Controlled human infection models in COVID-19 and tuberculosis: current progress and future challenges, Front. Immunol. 14 (2023) 1211388.

[3] E.A. Tarim, M.A. Inevi, I. Ozkan, S. Kecili, E. Bilgi, M.S. Baslar, E. Ozcivici, C. O. Karakus, H.C. Tekin, Microfluidic-based technologies for diagnosis, prevention, and treatment of COVID-19: recent advances and future directions, Biomed. Microdevices 25 (2) (2023) 10.

[4] N.N. Cheng, M.Z. Liu, W.T. Li, B.Y. Sun, D.D. Liu, G.Q. Wang, J.W. Shi, L.S. Li, Protein post-translational modification in SARS-CoV-2 and host interaction, Front. Immunol. 13 (2023) 1068449.

[5] J.V. Lazarus, K. Wyka, T.M. White, C.A. Picchio, L.O. Gostin, H.J. Larson, K. Rabin, S.C. Ratzan, A. Kamarulzaman, A. El-Mohandes, A survey of COVID-19 vaccine acceptance across 23 countries in 2022, Nat. Med. 29 (2023) 366–375.

[6] C.Y. Loo, W.H. Lee, Q.T. Zhou, Recent advances in inhaled nanoformulations of vaccines and therapeutics targeting respiratory viral infections, Pharm Res-dordr 40 (5) (2023) 1015–1036.

[7] P.K. Prabhakar, N. Khurana, M. Vyas, V. Sharma, G.E. Batiha, H. Kaur, J. Singh, D. Kumar, N. Sharma, A. Kaushik, R. Kumar, Aspects of nanotechnology for COVID-19 vaccine development and its delivery applications, Pharmaceutics 15 (2) (2023) 451.

[8] H.Q. Xu, H.Y. Li, H.L. You, P. Zhang, N. Li, N. Jiang, Y. Cao, L. Qin, G.X. Qin, H. B. Qu, H.Y. Wang, B. Zou, X. He, D. Li, H.Z. Zhao, G. Huang, Y. Li, H.F. Zhang, L. P. Zhu, H.M. Qiao, H.J. Li, S.R. Liu, L.N. Gu, G.D. Yin, Y. Hu, S.B. Xu, W.Y. Guo, N. Y. Wang, C.Y. Liu, P.J. Gao, J. Cao, Y. Zheng, K.Y. Zhang, Y. Wang, H. Chen, J. Zhang, D.M. Mu, J.Q. Niu, Effectiveness of inactivated COVID-19 vaccines against mild disease, pneumonia, and severe disease among persons infected with SARS-CoV-2 Omicron variant: real-world study in Jilin Province, China, Emerg. Microb. Infect. 12 (2023) 2149935.

[9] C. Stein, H. Nassereldine, R.J.D. Sorensen, J. Amlag, C. Bisignano, S. Byrne, E. Castro, K. Coberly, J.K. Collins, J. Dalos, F. Daoud, A. Deen, E. Gakidou, J. R. Giles, E.N. Hulland, B.M. Huntley, K.E. Kinzel, R. Lozano, A.H. Mokdad, T. Pham, D.M. Pigott, R.C. Reiner, T. Vos, S.I. Hay, C.J.L. Murray, S.S. Lim, Past SARS-CoV-2 infection protection against re-infection: a systematic review and meta-analysis, Lancet 401 (10379) (2023) 833–842.

[10] Z. Wang, K. Cui, U. Costabel, X. Zhang, Nanotechnology-facilitated vaccine development during the coronavirus disease 2019 (COVID-19) pandemic, Explorations 2 (2022) 20210082.

[11] C. Feng, P. Tan, G. Nie, M. Zhu, Biomimetic and bioinspired nano-platforms for cancer vaccine development, Explorations 3 (2023) 20210263.

[12] X.Y. Gao, Y.T. Xia, X.F. Liu, Y.L. Xu, P.Y. Lu, Z.P. Dong, J. Liu, G.F. Liang, A perspective on SARS-CoV-2 virus-like particles vaccines, Int. Immunopharm. 115 (2023) 109650.

[13] I. Ul Haq, K. Krukiewicz, G. Yahya, M. Ul Haq, S. Maryam, R.A. Mosbah, S. Saber, M. Alrouji, The breadth of bacteriophages contributing to the development of the phage-based vaccines for COVID-19: an ideal platform to design the multiplex vaccine, J. Mol. Sci. 24 (2) (2023) 1536.

[14] R. Das, R.N. Hyer, P. Burton, J.M. Miller, B.J. Kuter, Emerging heterologous mRNA-based booster strategies within the COVID-19 vaccine landscape, Hum. Vaccines Immunother. 19 (1) (2023) 2153532.

[15] K.D. Popowski, López de Juan Abad Blanca, A. George, D. Silkstone, E. Belcher, J. Chung, Inhalable exosomes outperform liposomes as mrna and protein drug carriers to the lung, Extracellular vesicle 1 (2022) 100002.

[16] Y. Sui, J. Li, J.Q. Qu, T. Fang, H.Y. Zhang, J. Zhang, Z.R. Wang, M.Y. Xia, Y.H. Dai, D.K. Wang, Dual-responsive nanovaccine for cytosolic delivery of antigens to boost cellular immune responses and cancer immunotherapy, Asian J. Pharm. Sci. 17 (4) (2022) 583–595.

[17] W. Ziqi, C. Kai, U. Costabel, Z.J.E. Xiaoju, Nanotechnology-facilitated vaccine development during the coronavirus disease 2019 (COVID-19) pandemic, Explorations 2 (2022) 20210082.

[18] P. Mayrhofer, M. Hunjadi, R. Kunert, Functional trimeric SARS-CoV-2 envelope protein expressed in stable CHO cells, Front. Bioeng. Biotechnol. 9 (2021) 779359.

[19] A.C. Walls, Y.J. Park, M.A. Tortorici, A. Wall, A.T. McGuire, D. Veesler, Structure, function, and antigenicity of the SARS-CoV-2 spike glycoprotein, Cell 183 (6) (2021) 1735.

[20] J.Y. Yu, N.D. Collins, N.B. Mercado, K. McMahan, A. Chandrashekar, J.Y. Liu, T. Anioke, A.Q. Chang, V.M. Giffin, D.L. Hope, D. Sellers, F. Nampanya, S. Gardner, J. Barrett, H.H. Wan, J. Velasco, E. Teow, A. Cook, A.V. Ry, L. Pessaint, H. Andersen, M.G. Lewis, C. Hofer, D.S. Burke, E.K. Barkei, H.A.D. King, C. Subra, D. Bolton, K. Modjarrad, N.L. Michael, D.H. Barouch, Protective efficacy of gastrointestinal SARS-CoV-2 delivery against intranasal and intratracheal SARS-CoV-2 challenge in rhesus macaques, J. Virol. 96 (2) (2022) e0159.

[21] S. Ravichandran, G. Grubbs, J.J. Tang, Y. Lee, C. Huang, H. Golding, S. Khurana, Systemic and mucosal immune profiling in asymptomatic and symptomatic SARS-CoV-2-infected individuals reveal unlinked immune signatures, Sci. Adv. 7 (42) (2021) eabi6533.

[22] M. Ejemel, Q. Li, S.R. Hou, Z.A. Schiller, J.A. Tree, A. Wallace, A. Amcheslavsky, N. K. Yilmaz, K.R. Buttigieg, M.J. Elmore, K. Godwin, N. Coombes, J.R. Toomey, R. Schneider, A.S. Ramchetty, B.J. Close, D.Y. Chen, H.L. Conway, M. Saeed, C. Ganesa, M.W. Carroll, L.A. Cavacini, M.S. Klempner, C.A. Schiffer, Y. Wang, A cross-reactive human IgA monoclonal antibody blocks SARS-CoV-2 spike-ACE2 interaction, Nat Commum 11 (1) (2020) 4198.

[23] B. Kingstad-Bakke, W. Lee, S.S. Chandrasekar, D.J. Gasper, C. Salas-Quinchucua, T. Cleven, J.A. Sullivan, A. Talaat, J.E. Osorio, M. Suresh, Vaccine-induced systemic and mucosal T cell immunity to SARS-CoV-2 viral variants, P Natl Acad Sci. USA 119 (2022) e211831211.

[24] F.L. Feng, Z.Y. Wen, J.S. Chen, Y. Yuan, C.C. Wang, C.J. Sun, Strategies to develop a mucosa-targeting vaccine against emerging infectious diseases, Viruses-Basel. 14 (3) (2022) 520.

[25] A.O. Hassan, N.M. Kafai, I.P. Dmitriev, J.M. Fox, B.K. Smith, I.B. Harvey, R. E. Chen, E.S. Winkler, A.W. Wessel, J.B. Case, E. Kashentseva, B.T. McCune, A. L. Bailey, H.Y. Zhao, L.A. VanBlargan, Y.N. Dai, M.S. Ma, L.J. Adams, S. Shrihari, J. E. Danis, L.E. Gralinski, Y.J. Hou, A. Schafer, A.S. Kim, S.P. Keeler, D. Weiskopf, R. S. Baric, M.J. Holtzman, D.H. Fremont, D.T. Curiel, M.S. Diamond, A single-dose intranasal Chad vaccine protects upper and lower respiratory tracts against SARS-CoV-2, Cell 183 (1) (2020) 169–184.

[26] L.C. Xiao, W.L. Yu, L.J. Shen, W.Y. Yan, J.M. Qi, T. Hu, Mucosal SARS-CoV-2 nanoparticle vaccine based on mucosal adjuvants and its immune effectiveness by intranasal administration, Acs Appl Mater Inter 15 (30) (2023) 35895–35905.

[27] K. Rakhra, W. Abraham, C.S. Wang, K.D. Moynihan, N. Li, N. Donahue, A. D. Baldeon, D.J. Irvine, Exploiting albumin as a mucosal vaccine chaperone for robust generation of lung-resident memory T cells, Sci. Immunol. 6 (57) (2021) eabd800.

[28] Y.F. Sun, J. Pi, J.F. Xu, Emerging role of exosomes in tuberculosis: from immunity regulations to vaccine and immunotherapy, Front. Immunol. 12 (2021) 628973.

[29] L.M. Doyle, M.Z. Wang, Overview of extracellular vesicles, their origin, composition, purpose, and methods for exosome isolation and analysis, Cells-Basel 8 (7) (2019) 72.

[30] M.F.S. Lindenbergh, W. Stoorvogel, Antigen presentation by extracellular vesicles from professional antigen-presenting cells, Annu. Rev. Immunol. 36 (2018) 435–459.

[31] L. Macia, R. Nanan, E. Hosseini-Beheshti, G.E. Grau, Host- and microbiota-derived extracellular vesicles, immune function, and disease development, Int. J. Mol. Sci. 21 (1) (2020) 107.

[32] N. Trevaskis, L. Kaminskas, C. Porter, From sewer to saviour - targeting the lymphatic system to promote drug exposure and activity, Nat. Rev. Drug Discov. 14 (11) (2015) 781–803.

[33] P. Kurywchak, J. Tavormina, R. Kalluri, The emerging roles of exosomes in the modulation of immune responses in cancer, Genome Med. 10 (2018) 23.

[34] M. Samuel, S. Gabrielsson, Personalized medicine and back-allogeneic exosomes for cancer immunotherapy, J. Intern. Med. 289 (2) (2021) 138–146.

[35] S. Wang, F. Li, T. Ye, J.H. Wang, C.L. Lyu, S. Qing, Z.W. Ding, X.Y. Gao, R.R. Jia, D. Yu, J. Ren, W. Wei, G.H. Ma, Macrophage-tumor chimeric exosomes accumulate in lymph node and tumor to activate the immune response and the tumor microenvironment, Sci. Transl. Med. 13 (2021) eabb6981.

[36] S. Jahan, S. Mukherjee, S. Ali, U. Bhardwaj, R.K. Choudhary, S. Balakrishnan, A. Naseem, S.A. Mir, S. Banawas, M. Alaidarous, H. Alyenbaawi, D. Iqbal, A. J. Siddiqui, Pioneer role of extracellular vesicles as modulators of cancer initiation in progression, drug therapy, and vaccine prospects, Cells-Basel 11 (3) (2022) 490.

[37] Andre Fabrice, Nathalie, et al., Exosomes as potent cell-free peptide-based vaccine. I."Exosomes as potent cell-free peptide-based vaccine.I.dendritic cell-derived exosomes transfer functional MHC class I/peptide complexes to dendritic cells", J. Immunol. 172 (4) (2004) 2126–2136.

[38] Z.Z. Wang, K.D. Popowski, D.S. Zhu, B.L.D. Abad, X.Y. Wang, M.R. Liu, H. Lutz, N. De Naeyer, C.T. DeMarco, T.N. Denny, P.U.C. Dinh, Z.H. Li, K. Cheng, Exosomes decorated with a recombinant SARS-CoV-2 receptor-binding domain as an inhalable COVID-19 vaccine, Nat. Biomed. Eng. 6 (7) (2022) 791–805.

[39] K.D. Popowski, A. Moatti, G. Scull, D. Silkstone, H. Lutz, B.L.D. Abad, A. George, E. Belcher, D.S. Zhu, X. Mei, X. Cheng, M. Cislo, A. Ghodsi, Y.H. Cai, K. Huang, J. L. Li, A.C. Brown, A. Greenbaum, P.U.C. Dinh, K. Cheng, Inhalable dry powder mRNA vaccines based on extracellular vesicles, Matter 5 (9) (2022) 2960–2974.

[40] W.T. Yang, G.L. Yang, Q. Wang, H.B. Huang, Y.L. Jiang, C.W. Shi, J.Z. Wang, K. Y. Huang, Y.B. Jin, C.F. Wang, Protective efficacy of Fc targeting conserved influenza virus M2e antigen expressed by Lactobacillus plantarum, Antivir. Res. 138 (2017) 9–21.

[41] Z.L. Li, X.Y. Zhou, X.T. Gao, D.N. Bai, Y. Dong, W.Q. Sun, L.B. Zhao, M.Y. Wei, X. K. Yang, G.D. Yang, L.J. Yuan, Fusion protein engineered exosomes for targeted degradation of specific RNAs in lysosomes: a proof-of-concept study, J. Extracell. Vesicles 9 (1) (2020) 1816710.

[42] K. Lederer, D. Castano, D.G. Atria, T.H. Oguin, S. Wang, T.B. Manzoni, H. Muramatsu, M.J. Hogan, F. Amanat, P. Cherubin, K.A. Lundgreen, Y.K. Tam, S. H.Y. Fan, L.C. Eisenlohr, I. Maillard, D. Weissman, P. Bates, F. Krammer, G. D. Sempowski, N. Pardi, M. Locci, SARS-CoV-2 mRNA vaccines foster potent antigen-specific germinal center responses associated with neutralizing antibody generation, Immunity 53 (6) (2020) 1281–1295.

[43] J. Kulkarni, D. Witzigmann, S. Chen, P. Cullis, R. van der Meel, Lipid nanoparticle technology for clinical translation of siRNA therapeutics, Accounts Chem. Res. 52 (9) (2019) 2435–2444.

[44] D. Vllasaliu, C. Alexander, M. Garnett, M. Eaton, S. Stolnik, Fc-mediated transport of nanoparticles across airway epithelial cell layers, J. Contr. Release 158 (3) (2012) 479–486.

[45] D. Luo, X. Yang, T. Li, N. Ning, S. Jin, Z. Shi, H. Gu, D. Li, Y. Gao, H. Wang, An updated RBD-Fc fusion vaccine booster increases neutralization of SARS-CoV-2 Omicron variants, Signal Transduct. Tar. 7 (1) (2022) 327.

[46] M. Nizard, H. Roussel, M.O. Diniz, S. Karaki, T. Tran, T. Voron, E. Dransart, F. Sandoval, M. Riquet, B. Rance, E. Marcheteau, E. Fabre, M. Mandavit, M. Terme, C. Blanc, J.B. Escudie, L. Gibault, F. Le Pimpec Barthes, C. Granier, L.C.S. Ferreira, C. Badoual, L. Johannes, E. Tartour, Induction of resident memory T cells enhances the efficacy of cancer vaccine, Nat. Commun. 8 (2017) 15221.

[47] N. Stapleton, H. Einarsdóttir, A. Stemerding, G.J. I.r. Vidarsson, The multiple facets of FcRn in immunity, Immunol. Rev. 268 (1) (2015) 253–268.

[48] D. Castaneda, C. Dhommée, T. Baranek, E. Dalloneau, L. Lajoie, A. Valayer, C. Arnoult, M. Demattéi, D. Fouquenet, C. Parent, N. Heuzé-Vourc'h, V.J. F.i. i. Gouilleux-Gruart, Lack of FcRn impairs natural killer cell development and functions in the tumor microenvironment, Front. Immunol. 9 (2018) 2259.

[49] V. Sharma, C.D. Mukhopadhyay, Exosome as drug delivery system: current advancements, Extracellular Vesicle 3 (2024) 100032.

[50] J.M. Pitt, André Fabrice, S. Amigorena, J.C. Soria, L. Zitvogel, Dendritic cell–derived exosomes for cancer therapy, J. Clin. Invest. 126 (4) (2016) 1224.

[51] Y. Xinyu, C. Jiale, W. Ning, et al., Clinical use of dendritic cell-derived exosomes for hepatocellular carcinoma immunotherapy: how far we are? J. Hepatol. 69 (2018) 984–986.

[52] R. Heida, W. Hinrichs, H. Frijlink, Inhaled vaccine delivery in the combat against respiratory viruses: a 2021 overview of recent developments and implications for COVID-19, Expert, Rev. Vaccines. 21 (7) (2021) 957–974.
[53] T. Mao, B. Israelow, M. Peña-Hernández, A. Suberi, L. Zhou, S. Luyten, M. Reschke, H. Dong, R. Homer, W. Saltzman, A. J. S. Iwasaki, Unadjuvanted intranasal spike vaccine elicits protective mucosal immunity against sarbecoviruses, Science. 378 (6622), eabo2523.
[54] O. Alfi, A. Yakirevitch, O. Wald, O. Wandel, U. Izhar, E. Oiknine-Djian, Y. Nevo, S. Elgavish, E. Dagan, O. Madgar, G. Feinmesser, E. Pikarsky, M. Bronstein, O. Vorontsov, W. Jonas, J. Ives, J. Walter, Z. Zakay-Rones, M. Oberbaum, A. Panet, D. G. Wolf, J. Virol. 95 (14), e00130-21.
[55] Z. Wang, K. Popowski, D. Zhu, B. de Juan Abad, X. Wang, M. Liu, H. Lutz, N. De Naeyer, C. DeMarco, T. Denny, P. Dinh, Z. Li, K.J. N.b. e. Cheng, Exosomes decorated with a recombinant SARS-CoV-2 receptor-binding domain as an inhalable COVID-19 vaccine, Nat. Biomed. Eng. 6 (7) (2022) 791–805.
[56] C. Charoenviriyakul, Y. Takahashi, M. Nishikawa, Y. Takakura, Preservation of exosomes at room temperature using lyophilization, Int. J. Pharm. (Amst.) 553 (1–2) (2018) 1–7.